Nano-functional Photonics Research Team

Team Leader : Satoshi Kawata

Unpublished results are not included.

Frequency dependence of the magnetic response of split-ring resonators

A. Ishikawa, T. Tanaka, and S. Kawata,
J. Opt. Soc. of Am. B 24 (2007) 510-515.

The design principle of split-ring resonators (SRRs) for realizing negative magnetic metamaterial is proposed through theoretical investigation of magnetic properties of SRRs from terahertz (THz) to the visible light region. To describe the frequency dispersion of metal throughout the frequency range, we consider the exact expression of the internal impedance formula. Our results indicate that the design principle should be changed completely at the transition frequency of 100 THz. Below 100 THz, since the resistance of the SRRs determines the magnetic responses, low-resistance structures are essential. On the other hand, we should design the SRRs' structures maintaining large geometrical inductance above the 100 THz region, because the decrease of the geometrical inductance dominantly reduces the magnetic responses.

The investigation provides a design strategy for plasmonic metamaterials which provide magnetic response in the visible light region and may lead to new optical functional materials in the optics and photonics field.

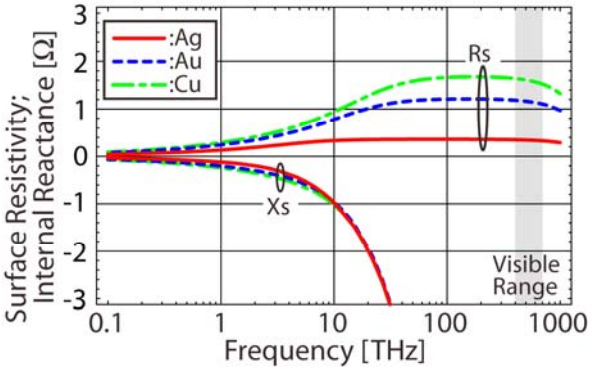

Fig.1 Dispersion curves of the internal impedance of silver, gold, and copper; Rs: surface resistivity; Xs: internal reactance

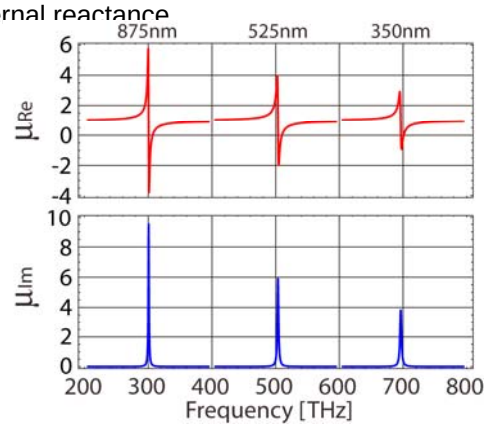

Fig 3. Real and imaginary parts of the effective permeability of silver s-SRRs as a function of the s-SRRs' dimensions.

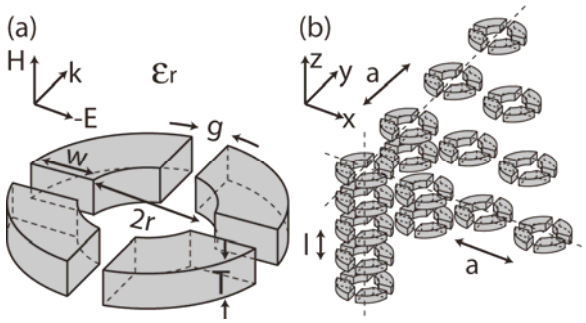

Fig 2. Models of single s-SRR used in calculations above100 THz. (a) Element of the s-SRR and (b) array of the s-SRRs

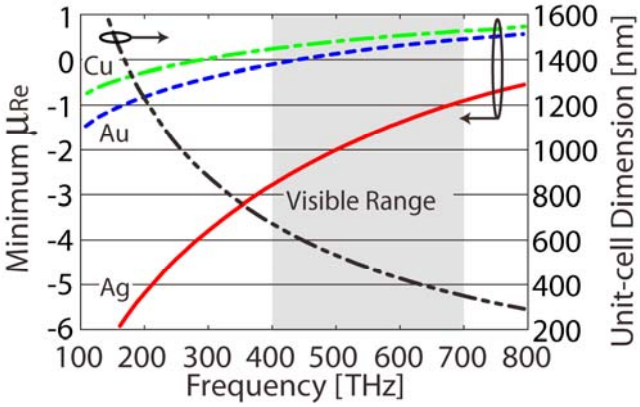

Fig 4. Frequency dependencies of the minimum μ_{Re} of the s-SRRs made of silver, gold, and copper.

Magnetic excitation of magnetic resonance in metamaterials at far-infrared frequencies

A. Ishikawa, T. Tanaka, and S. Kawata, Appl. Phys. Lett. 91 (2007) 113118.

The authors experimentally demonstrated magnetically excited magnetic resonances with negative magnetic permeability in a metamaterial composed of an array of silver rod pairs. In transmission spectroscopy of the metamaterial, by employing oblique incidence, an incidentmagnetic-field-dependent absorption feature was clearly observed at 18 THz. The experimental results directly prove that the rod pair structure interacted with the magnetic field of the incident light, producing magnetic resonance. The experimental results were in good agreement with a numerical simulation suggesting that the value of ┌Re of the silver rod pair array changes from ─0.29 to 2.26 at resonance.

This investigation demonstrated magnetic excitation of magnetic resonances in a metamaterial composed of an array of silver rod pairs by employing transmission spectroscopy with oblique incidence. It may lead to new plasmonic metamaterial structure as an artificially magnetic materials.

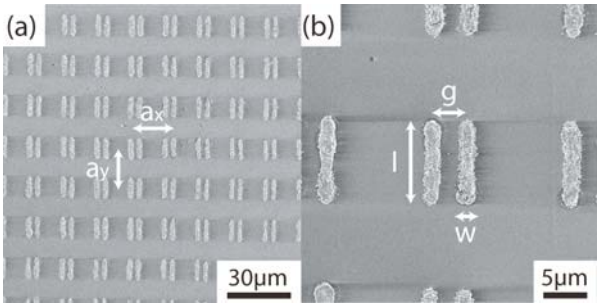

Fig 1. (a) SEM image of silver rod pair array fabricated on a quartz substrate and (b) its magnified image.

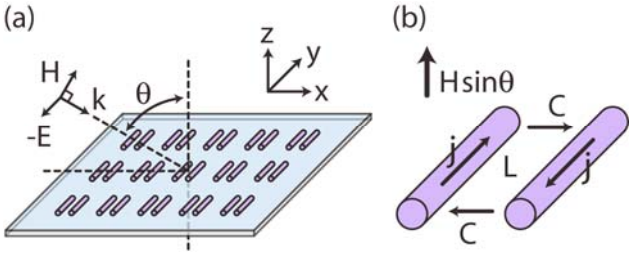

Fig 2. Optical setup for measuring the magnetically excited magnetic responses of the rod pair array by changing the incident angle (θ) of s-polarized light.

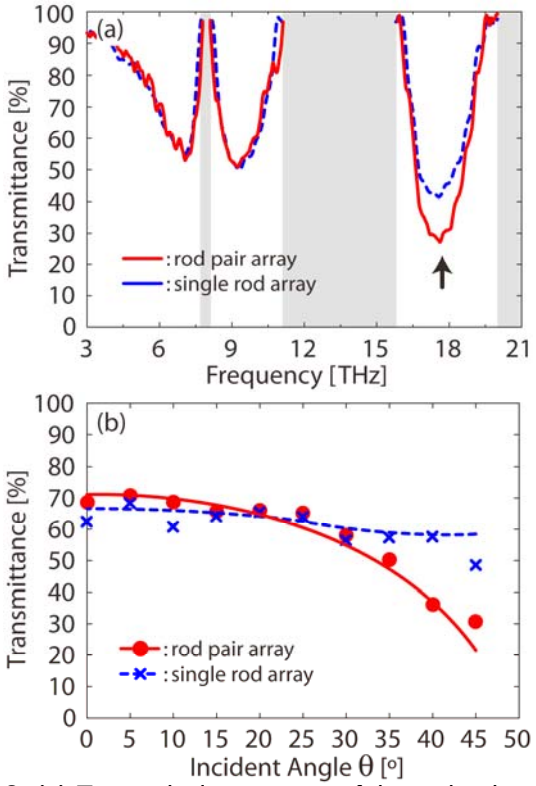

Fig 3. (a) Transmission spectra of the rod pair array and the single (unpaired) rod array measured at θ = 45º. (b) Incident angle dependencies of the transmittances of the rod pair array and the single rod array measured at 18 THz.

Improving spatial resolution of two-photon microfabrication by using photoinitiator with high initiating efficiency

J.F. Xing, X.Z. Dong, W.Q. Chen, X.M. Duan, N. Takeyasu, T. Tanaka, and S. Kawata, *Appl. Phys. Lett.* 90 (2007) 131106.
J.F. Xing, W.Q. Chen, J. Gu, X.Z. Dong, N. Takeyasu, T. Tanaka, X.M. Duan, and S. Kawata, *J. Mater. Chem.* 17 (2007) 1433.
J.F.Xing, W.Q.Chen, X.Z. Dong, T. Tanaka, X.Y. Fang, X.M. Duan, and S. Kawata, *J. Photochem. Photobio.* A 189 (2007) 398.

Laser stereolithography based on two-photon induced polymerization (TPIP) has been established as a powerful tool for three-dimensional micro-and nano-fabrications. The lateral spatial resolution (LSR) in TPIP was improved to 80 nm by using an anthracene derivative (BPDPA) as a highly sensitive and efficient photoinitiator (Fig. 1 and 2). Photocurable resin containing 0.18 mol% BPDPA exhibited a lower polymerization threshold of 0.64 mW at 800nm. LSR was also investigated with different types of photoinitiators, which were a carbazole derivative (Fig. 3) and anthraquinone derivatives (Fig. 4).

Our results indicate that the photoinitiator with high initiating efficiency results in a low polymerization threshold, which is advantageous for improving the lateral spatial resolution. The fabrication resolution in TPIP could be improved using more sensitive photoinitiators.

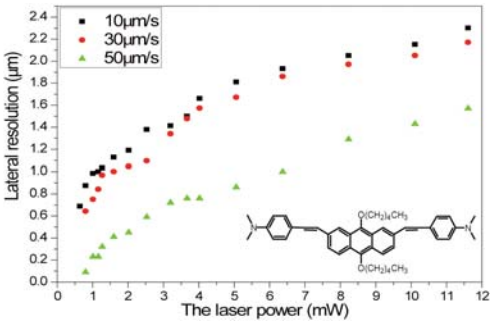

Fig 1. Relationship between LSR and laser power at different linear scan speeds for anthracene derivative.

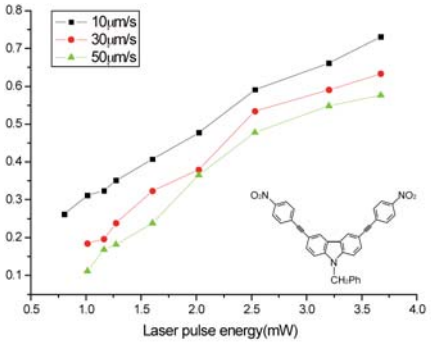

Fig 3. Relationship between LSR and laser power at different linear scan speeds for carbazole derivative.

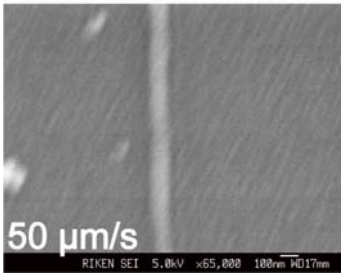

Fig 2. SEM image of the polymer line (80nm) fabricated by using a laser power of 0.8 mW and a linear scan speed of 50 μm/s.

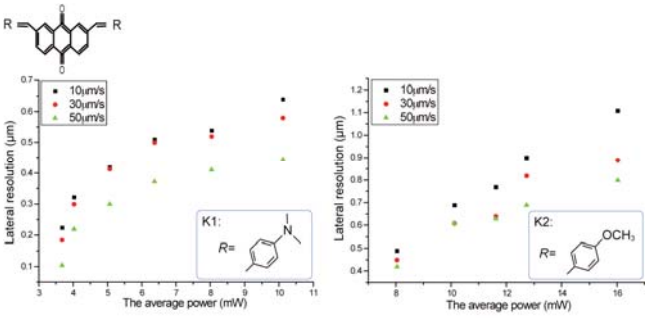

Fig 4. Relationship between LSR and laser power at different linear scan speeds for anthoraquinone derivatives (K1 and K2).

Fabrication of 3D metal/polymer microstructures by site-selective metal coating

N. Takeyasu, T. Tanaka, and S. Kawata, *Appl. Phys.* A 90 (2008) 205.

Three-dimensional silver/polymer conjugated microstructures were fabricated by site-selective metal deposition on photopolymer structures in the sub-micrometer scale. Photopolymerizable resins with and without an amide group were independently prepared (Fig. 1), and a three-dimensional polymer structure was fabricated with those resins by means of two-photon induced photopolymerization technique to confine the photopolymerization to a sub-micrometer volume. Silver was selectively deposited on the surface of the amide-containing polymer parts by electroless plating (Fig. 2). This method can provide 3D arbitrary silver/polymer composite microstructures with sub-micrometer resolution (Fig. 3).

Our results show that the 3D metal/ polymer microstructures can be fabricated by using the technique introduced here. It is expected to enable fabrication of arbitrary shaped 3D aligned metallic structures.

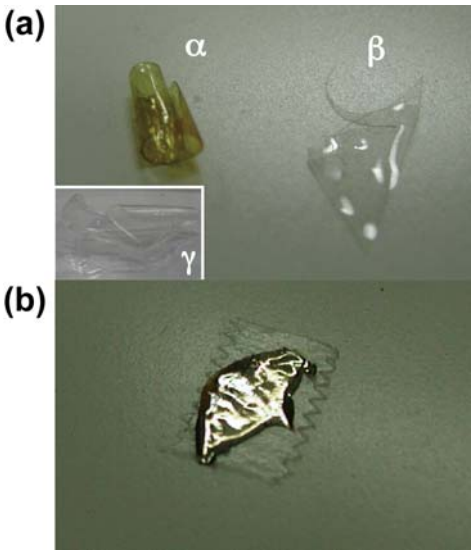

Fig. 1 (a) polymer films from the activated (α) and non-activated (β) resin after soaking for 24 h in the Ag solution; the inset (γ) shows polymerized film made from activated resin UV irradiation; (b) the activated polymer film after silver deposition by electroless plating.

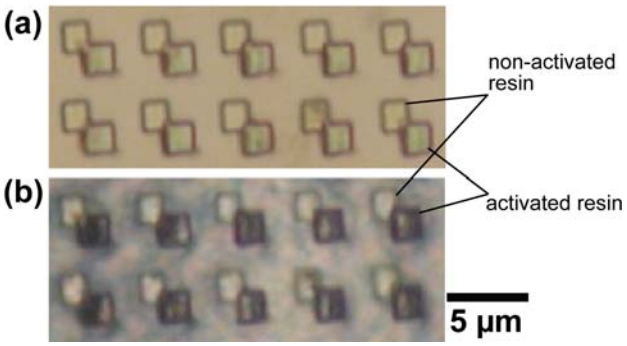

Fig 2. Microscope images of pairs of polymer sheets made by TPIP with the non-activated resin and the activated resin after (a) soaking in Ag solution for 6 h; and (b) electroless plating. The size of each square sheet is 2 μm by 2 μm.

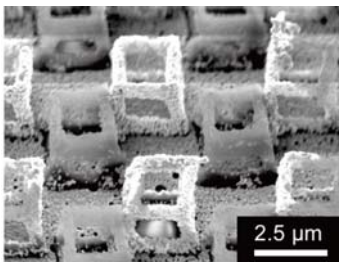

Fig 3. SEM image of silver/ polymer 3D microstructures.

3D Metallic Nano-Structure Fabrication By Surfactant-Assisted Multi-Photon-Induced Reduction

Y.-Y. Cao, N. Takeyasu, T. Tanaka, X.-M. Duan, and S. Kawata
***Small* 5 (2009) 1144.**

A laser fabrication technique for metal nanostructures is developed. We present a means to gain small feature size in the fabrication of metallic structures with the aid of a surfactant as a metal growth inhibitor. The minimum size of the silver structure fabricated by the proposed method was finer than the diffraction limit of light. For the first time, a feature size as small as 120 nm was also realized for 2D silver patterns on the substrate (Fig. 1). We also demonstrated that the feature size was reduced to 180 nm for 3D structures by laser fabrication (Fig. 2). We also proposed to illustrate the mechanism for nanometer scale patterning of metallic structures in multi-photon-induced reduciton technique, and show how the growth inhibiting effect of a surfactant aids in the nano-pattering of metallic nanostructures experimentally.

Our results may open the way to create arbitrary 3D metal structures with 100 nm resolution and investigate unique functions of 3D metal structures in the nano-scale world.

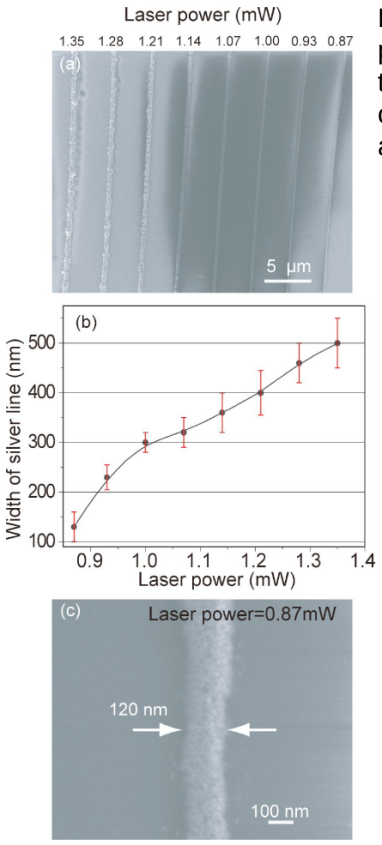

Fig. 1 (a) SEM image of silver stripe patterns formed using different laser powers and a linear scanning speed of 6μm/s. (b) Relationship between the laser power and width of the silver line from (a). (c) Magnified image of a silver line (width 120nm) fabricated using a laser power of 0.87 mW and a linear scanning speed of 6 μm/s.

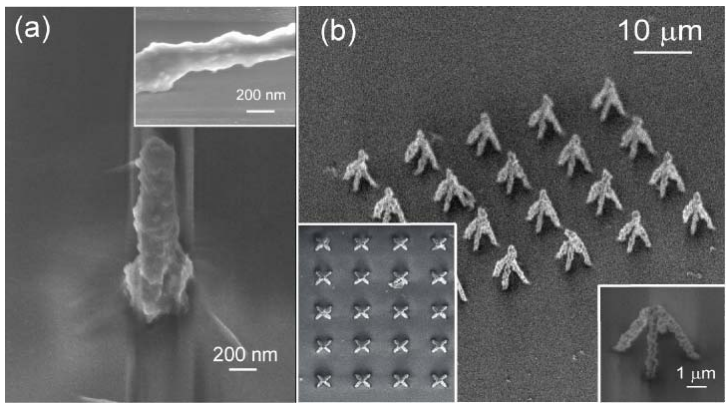

Fig. 2 (a) SEM image of the free-standing silver pillar on the cover slip, made by using a laser power of 1.14 mW and a linear scanning speed of 3 μm/s. The inset is a close-up view of the silver pillar parallel to the substrate, which demonstrates the resolution of the silver pillar as 180 nm. (b) SEM image of silver pyramids, fabricated with a laser power of 1.3 mW and scanning speed of 2.5 μm/s. The inset on the left is a top view of the silver-pyramid array. The inset on the right is a close-up view of the silver pyramid.

Plasmonic crystal for efficient energy transfer from fluorescent molecules to long-range surface plasmons

T. Okamoto, J. Simonen, and S. Kawata, *Opt. Express* 16 (2009) 8294 .

Corrugated metallic thin film structures that do not support short-range surface plasmon modes but do support long-range modes are discussed. The coupling efficiency of the energy of excited fluorescent molecules to long-range modes is theoretically calculated using the rigorous coupled wave approach. The obtained maximum coupling efficiency is found to be 55%, more that two times higher than the efficiency of uncorrugated metallic thin films.

The investigation provides the energy coupling efficiency from excited molecules to surface plasmons and may lead to optimal structures for plasmonic lasers and organic light emitting devices.

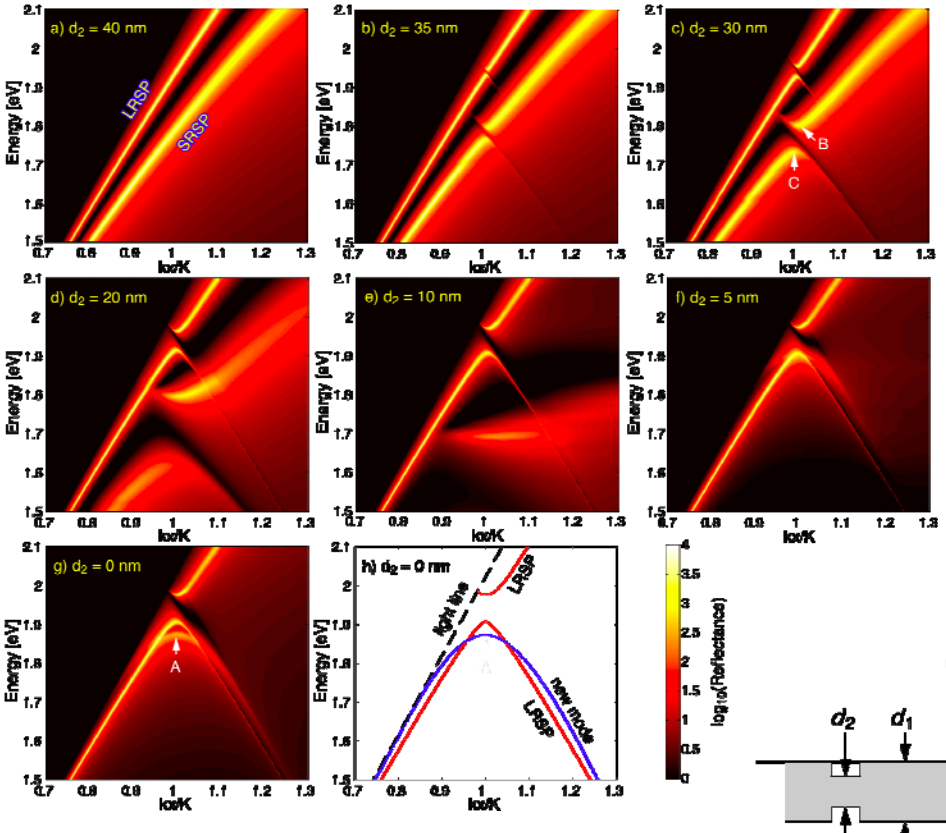

Fig 1. (a)-(g): Efficiency of the reflected zeroth order diffraction by the corrugated thin silver films with different minimum film thicknesses d_2 and (h): the loci of the reflection maxima shown in (g) to clarify the existing modes.

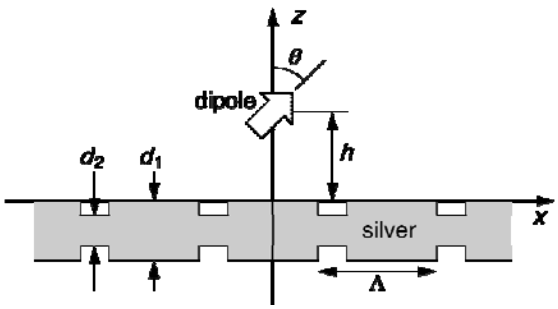

Fig 2. Geometry of the calculated model. There is no variation in the *y*-direction. The ambient is assumed to be Alq_3 doped with DCM with a dielectric constant of ε_1=2.89. The fill factor of the grating is 75%.

Enhancement of surface plasmon-mediated radiative energy transfer through a corrugated metal cathode in organic light-emitting

J. Feng, T. Okamoto, R. Naraoka, and S. Kawata, *Appl. Phys. Lett.* 93 (2008) 051106.

We report enhanced top emission from organic light-emitting devices by surface plasmon-mediated radiative energy transfer. A dye-doped dielectric acceptor layer was deposited onto the surface of a one-dimensionally corrugated silver cathode and was excited by the electroluminescence of a donor layer, which is located at the other side of the cathode. Ten times enhancement in emission intensity from the acceptor was observed compared to flat devices; this is due to the enhanced radiative energy transfer from the donor to the acceptor by the coupled surface plasmons on the opposite interfaces of the silver cathode.

The investigation provides efficient energy-transfer emission through a metallic cathode in organic light-emitting devices and may lead to a method to realize full color top-emitting organic light-emitting devices.

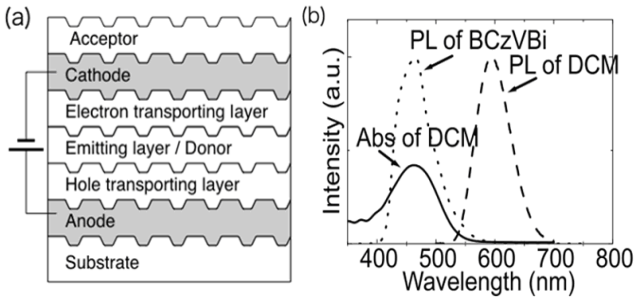

Fig 1. (a) Configuration of the corrugated device structure. (b) PL spectrum of BCzVBi and PL and absorption spectra of DCM-doped BCP (10% wt).

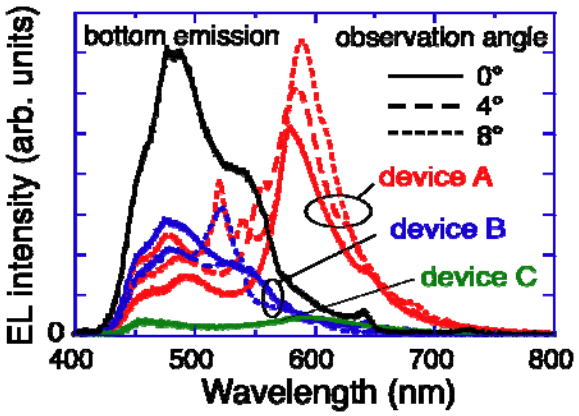

Fig 2. EL spectra observed from the topside of the device shown in Fig. 1 (device A), the same device but without acceptor (device B), the same device but without corrugation (device C), and from bottom side of the device A at normal direction.

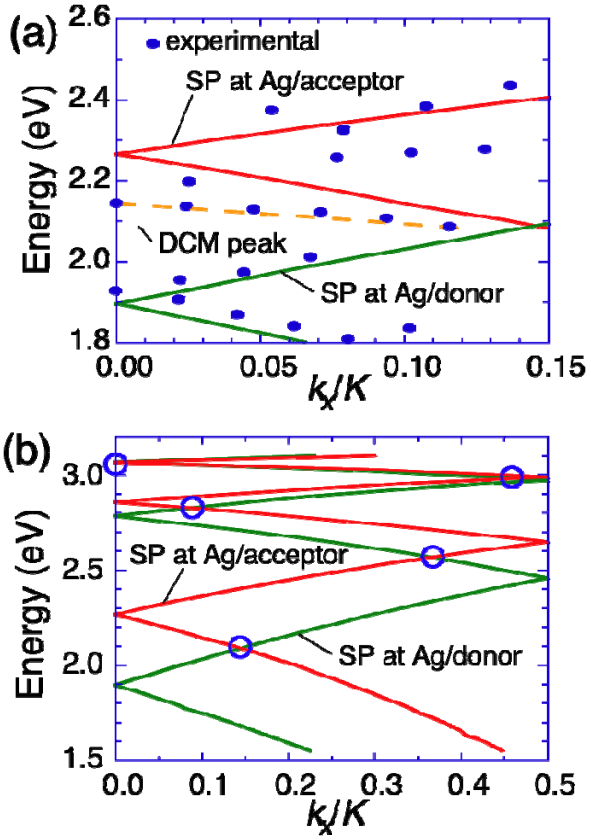

Fig 3. (a) Calculated dispersion relation for the structure of BCzVBi (semi-infinite)/ BCP(20 nm)/Ag (40 nm)/BCP (40 nm)/air and the dispersion relation obtained from the emission peaks of the EL spectra observed from the topside of the device A. (b) Calculated dispersion relation for the same structure in a wider energy and wave vector region.

Plasmonic band gaps of structured metallic thin films evaluated for a surface plasmon laser using the coupled-wave approach

T. Okamoto, J. Simonen, and S. Kawata, *Phys. Rev. B.* 77 (2008) 115425.

The behavior of plasmonic band gaps appearing in the dispersion relations of surface plasmons for periodically corrugated thin silver films is theoretically investigated by using the rigorous coupled-wave approach. The structures have one-dimensional rectangular corrugations with 25%, 50%, and 75% fill factors and support both long-range and short-range surface plasmon band gaps. A unified explanation for the necessary conditions for opening these band gaps, as well as intermode band gaps, is given. The radiation characteristics of the surface plasmons at the edges of these band gaps are also analyzed. Based on the findings, the optimal structure for a plasmonic band gap laser is presented.

The investigation provides optical properties of plasmonic-crystal thin-films on which both surfaces are periodically corrugated and may lead to optimal structures for plasmonic lasers, which require low absorption and radiation loss.

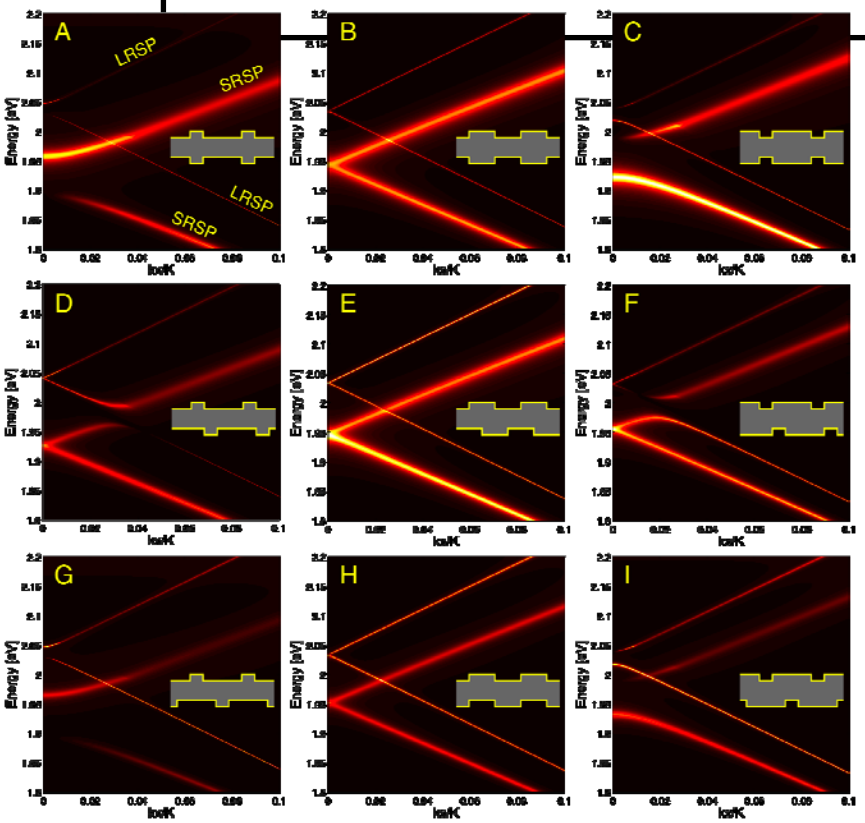

Fig 1. Examples of the calculated dispersion relations for various structures; normalized absorptance as a function of the energy E and the in-plane wave vector k_x of incident light. The insets indicate the film structures. The fill factors of the corrugation in both interfaces are identical. The incidence is from above. Two intramode bandgaps open for structures A, C, G, and I, while intermode bandgap opens for structures D and F. There are very narrow gaps at k_x=0 in structures B and H, but no gap in structure E.

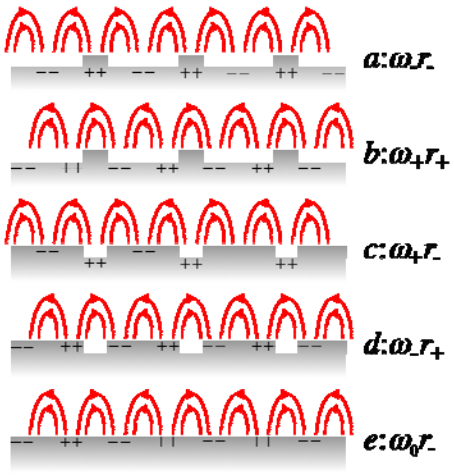

Fig 2. Charge distribution for standing surface plasmons in corrugated and uncorrugated metal surfaces of semi-infinite thick metals.

Color-tunable electroluminescence from white organic light-emitting devices through coupled surface plasmons

J. Feng, T. Okamoto, J. Simonen, and S. Kawata,
***Appl. Phys. Lett.* 90 (2007) 081106.**

The authors report color-tunable electroluminescence from white organic light-emitting devices (WOLEDs) through coupling of surface plasmons in a metal/insulator/metal (MIM) structure. The MIM structure was fabricated by depositing Ag and 2, 9-dimethyl-4, 7-diphenyl-1, 10-phenanthroline (BCP) films on the Ag cathode of a WOLED. The transmission wavelength through the MIM structure depends on the thickness of the middle BCP layer and can be tuned in the visible range. Therefore, the broadband emission from WOLEDs is selectively transmitted, and color-tunable EL emission was obtained. Blue, green, and red light emissions were observed when the BCP layer thicknesses are 70, 100, and 130 nm, respectively.

The investigation provides color-tunable emission in the visible region with a metal-insulator-metal structure on the top of white organic light-emitting devices (OLEDs) and may lead to a method realizing full color top-emitting OLEDs.

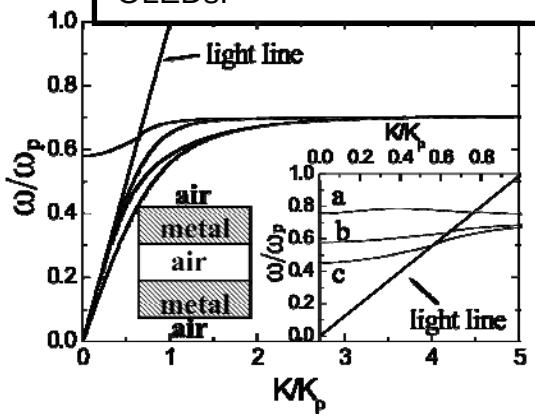

Fig 1. Dispersion relation of MIM structure in which the insulator region is air and is $0.5\lambda_p$ thick, and the thicknesses of two metal layers are both $0.25\lambda_p$, where $\lambda_p=2\pi c/\omega_p$ and ω_p is the plasma frequency. The frequency and the wave vector are normalized with respect to ω_p and k_p ($=\omega_p/c$); c is the speed of light in air. Inset shows the dispersion relation for the highest energy mode for air gaps of (a) $0.25\lambda_p$, (b) $0.5\lambda_p$, and (c) $0.75\lambda_p$.

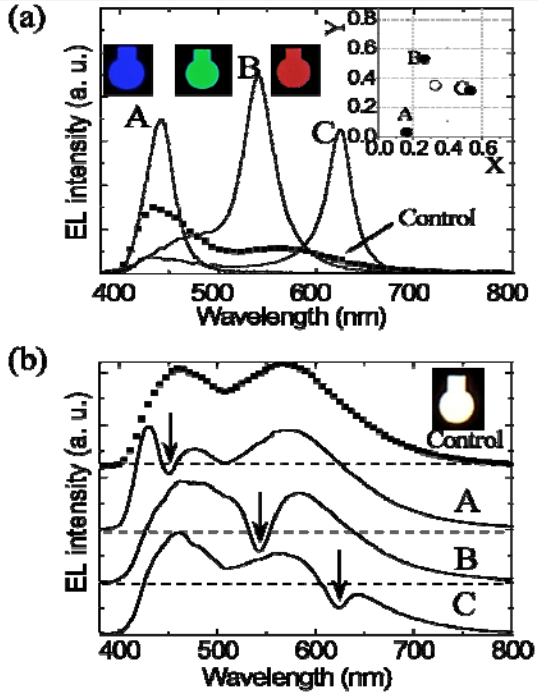

Fig 2. (a) EL spectra observed at normal direction from the top side of devices A (x=70nm), B (x=100nm), C (x=130nm), where x is the thickness of the middle BCP layer, and the control device (solid square). (b) EL spectra observed from the bottom side and normal direction of the same. The inset in (a) shows photographs of operating devices and CIE coordinates of devices A, B, and C. The inset in (b) shows a photograph of the operating control device.

Color Selection in Plasmon Holography

M. Ozaki, J. Kato, R. Furutani, and S. Kawata,
J. Jap. Soc. Prec. Eng. 74 (2008) 1113-1118.

Image reconstruction characteristics of the surface plasmon (SP) holography, which is composed of silver film supporting the SP propagation and hologram layer diffracting the SP wave, are investigated. From the viewpoint of the dependence on the SP hologram structures, a silver relief deposited on a dielectric hologram and a dielectric hologram placed on flat silver film are experimentally demonstrated and compared. The reconstructed image by silver relief hologram shows extremely high diffraction efficiency under He-Ne laser excitation even though the modulation depth of hologram is quite shallow. In white light reconstruction, it is found that the appropriate design of the structure makes it possible to control the color selectivity and also realize efficient white color reconstruction. The differences in the reconstruction properties are discussed in terms of the structural aspect of SP holography and SP excitation mechanisms.

This result is connected to realization of multi-color 3D display using the surface plasmon holography. (in preparation)

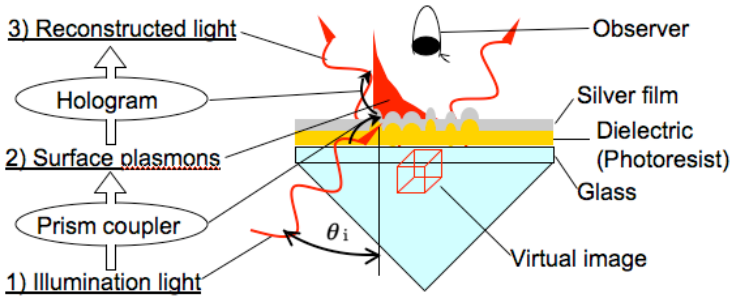

Fig. 1 Scheme of reconstruction of the silver surface-relief plasmon hologram. SPP excitation and hologram reconstruction simultaneously occur on the same surface.

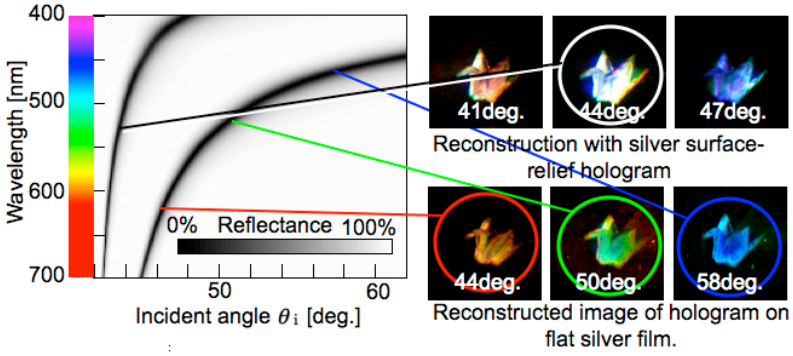

Fig.2 Chart: Dispersion relations calculated for two type of the SPP holograms as the reflectance in terms of the wavelength and the incident angles for exciting the SPPs. Reconstructed images for each type of holograms with collimated white light illuminations.

Three-Dimensional Multilayered Optical Memory Using Two-Photon Induced Reduction of Au^{3+} Doped in PMMA

T. Tanaka and S. Kawata

IEEE TRANSACTIONS ON MAGNETICS 43 (2007) pp. 828-831.

We developed a rhodamine-B and Au^{3+} doped PMMA medium for three-dimensional multilayered optical storage. Using the quenching of rhodamine-B by Au^{3+} ions and the two-photon induced reduction of Au^{3+} ions to the Au nanoparticle, the developed medium can record and store binary bit data in the form of a fluorescent patterns inside a thick medium. The recorded fluorescent pattern is read out three-dimensionally by using pick-up which incorporates confocal laser scanning fluorescent microscopy.

This research result provides a novel recording medium for three-dimensional multilayered optical memory. The material can store the bit data three-dimensionally as a fluorescent pattern and retrieved without any cross talks.

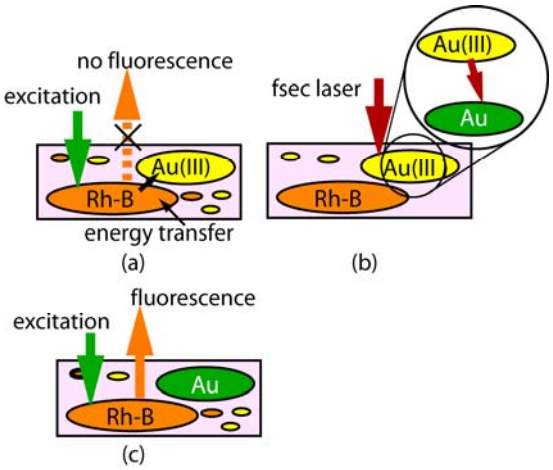

Fig 1. Recording mechanism of the fluorescent patterns inside the developed rhodamine-B and Au^{3+} doped PMMA medium.

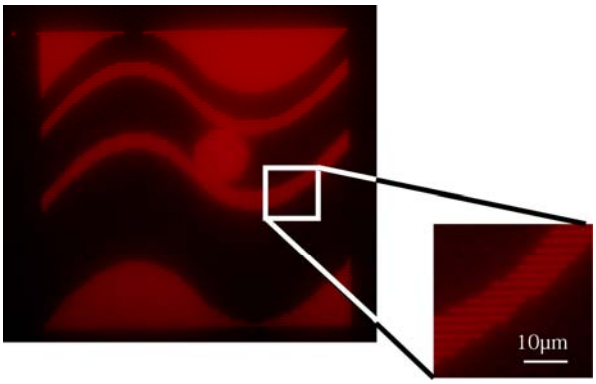

Fig 2. Experimental result of fluorescent pattern recording. Bright or white area emits fluorescence due to the reactivation by the reduction of Au^{3+} ions, while at the dark areas, rhodamin-B molecules are quenched by the Au^{3+} ions.

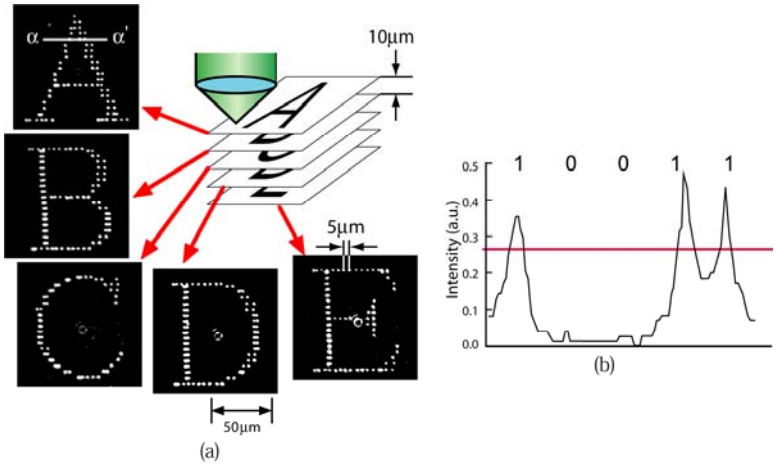

Fig. 3 Experimental result of three-dimensional recording.
(a) Five patterns “A”, “B”, “C”, “D”, and “E” were recorded with 10 μm longitudinal spacing.

Near-field temperature control for nanoscale fabrication/analysis

A. Tarun, N. Hayazawa, S. Kawata, Jpn. J. Appl. Phys. In press.
A. Tarun, M. Motohashi, N. Hayazawa, S. Kawata, Proc. SPIE, 7033 (2008) 70330C.

In near-field optical detection, the local temperature can be increased due to efficient tip-enhancement effect and highly confined photon density in a local volume. We calculated the local temperature at the tip apex under laser irradiation by finite element method and experimentally confirmed that the local temperature can be increased and controlled up to 1000K simply by varying the excitation laser power. This near-field thermal effect can be applicable either to analyses of thermal properties of materials or to fabrication in the nanoscale. We successfully demonstrate site-selective cutting of carbon nanotubes by laser heated near-field probe tip.

Further work is necessary to clarify the origin of the burnout and to determine the nature of heat transfer from tip to the nanotubes. Regardless of their origin and mechanism, the technique presented provides an alternative way of site-selective cutting to enable a broader set of applications of nanotubes to functional devices. The technique presented can also be extended to tip-heating assisted tip-enhanced Raman scattering for thermal characterization of various materials in the nanoscale.

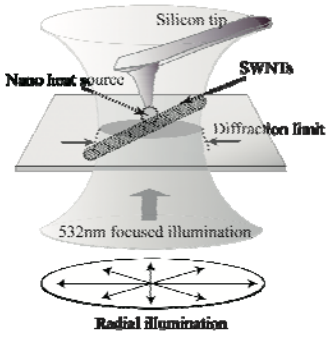

Fig 1. Experimental configuration used for selective cutting of nanotubes.

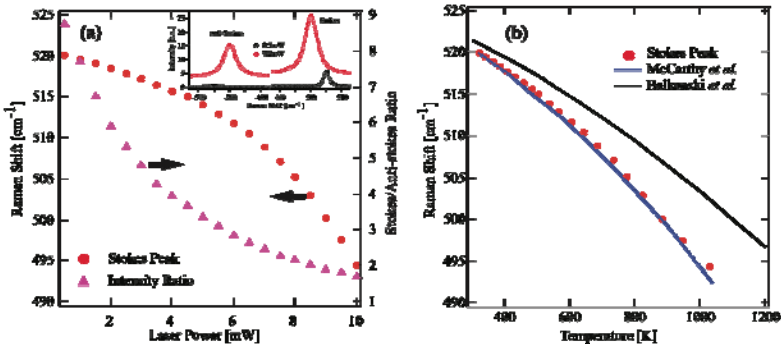

Fig 2. (a) Plot of the Raman shift in Si tip as a function of laser power. (b) Plot of Raman shift against the temperature calculated from the Stokes/anti-Stokes ratio.

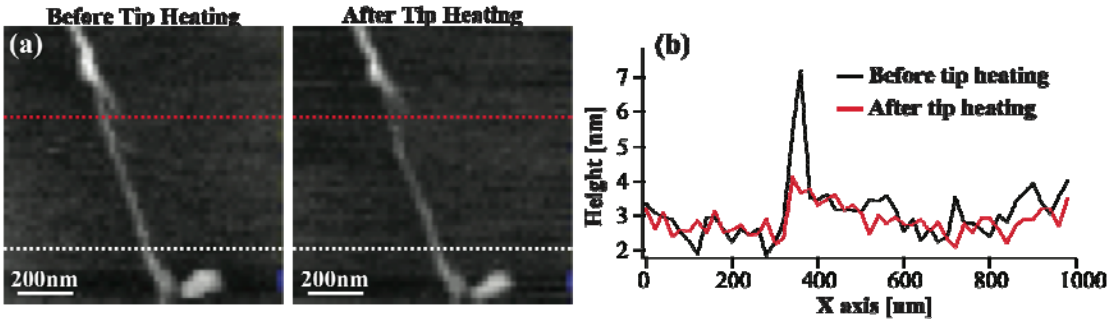

Fig 3 (a) AFM images before and after burnout. Image size is 1.0x1.0 μm^2 (50x50 pixels at 20 nm/pixel). Two different powers, 7 mW (white dashed line) and 9 mW (red dashed line) were used. (b) The cross-sectional profile at the red dashed line.

Nanomovement of azo polymers induced by metal tip enhanced near-field irradiation

H. Ishitobi, M. Tanabe, Z. Sekkat, and S. Kawata, Appl. Phys. Lett. 91 (2007) 091911.

Nanomovement of azo polymers induced by metal tip enhanced near-field illumination was studied. A protrusion with 47 nm full width at half maximum was induced with a resolution beyond the diffraction limit. At the top of the protrusion, an anisotropic movement occurs in a direction nearly parallel to the polarization of the incident light, and suggests the existence at the tip end of not only a longitudinal but also a lateral component of the electric field of light. The anisotropic photofluidity and the optical gradient force played important roles in the process of the light induced polymer movement.

The present work will trigger future studies addressing the fundamentals and theories of light induced polymer movement and can be applied to visualize the electric field distribution localized at a nano scale.

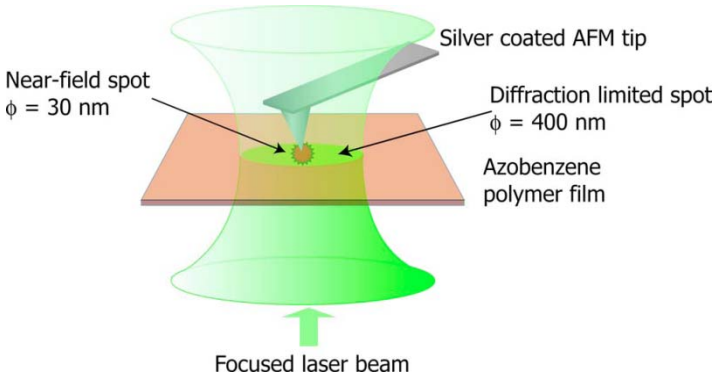

Fig 1. Schematic of the near-field surface deformation configuration.

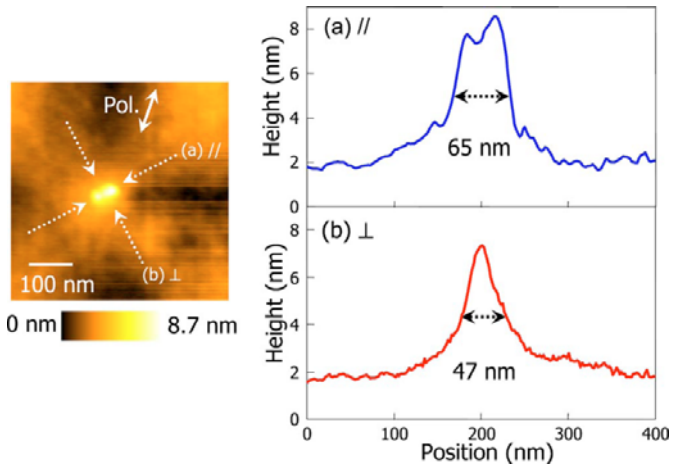

Fig 2. AFM image of the near-field surface deformation.

Mono-Domain Growth of Liquid-Crystalline Blue Phase and its Application to Photonic and Display Devices

K. Shirota, S. Kawata, Proc. IDW'09 (2009) LCT-2-2.

The blue phase (BP), one of the chiral liquid crystal phases is expected to play a role as photonic materials, as it forms three-dimensional cubic lattice structure. This higher-order photonic structure of the BP can make the threshold of laser oscillation lower than that of chiral nematic phases (N*). Problems of the BP for practical use are, however, its narrow temperature range and its inhomogeneous platelet texture. The lasing threshold of monodomain BP I at 52.3 ° C was observed to be half of the N*. For the purpose of expanding the temperature range of the BP and realizing the laser oscillation at room temperature, we applied a polymer-stabilization method. Resultant temperature range of the polymer-stabilized BP was expanded to over 50° C in width including the room temperature. The lasing threshold of the PSBP measured almost same as that of the unpolymerized BP.

Developed mono-domain polymer-stabilized blue phase, which does not require temperature control, may be useful for laser, waveguide and display applications.

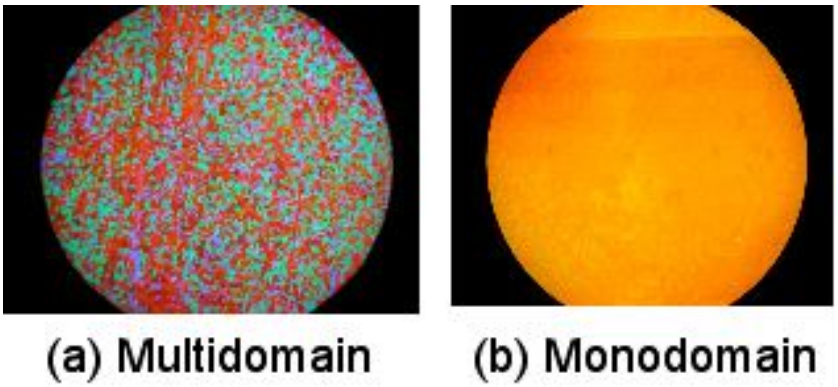

Fig. 1. Polarization micrographs of multidomain polmer-stabilized blue phase (a) and monodomain sample (b).

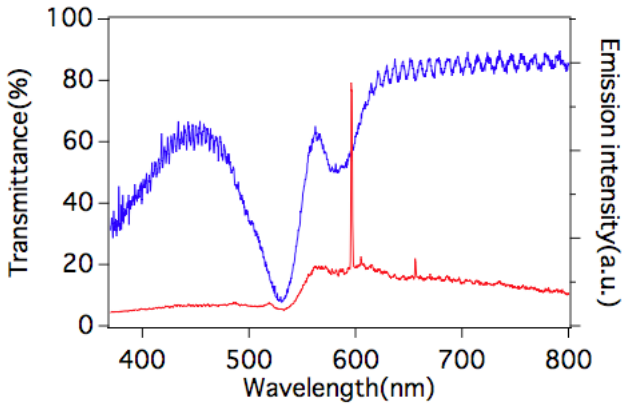

Fig 2. Transmission and emission spectra from monodomain polymer-stabilized blue phase.